Received 4 February 2023; accepted 28 February 2023. Date of publication 7 March 2023; date of current version 21 March 2023.

Digital Object Identifier 10.1109/OJCOMS.2023.3253643

Broadband Connectivity for Handheld Devices via LEO Satellites: Is Distributed Massive MIMO the Answer?

MOHAMMED Y. ABDELSADEK [1,2] (Senior Member, IEEE), GUNES KARABULUT-KURT [3,4] (Senior Member, IEEE), HALIM YANIKOMEROGLU [1] (Fellow, IEEE), PENG HU [5] (Senior Member, IEEE), GUILLAUME LAMONTAGNE [6], AND KHALED AHMED [6]

[1] Non-Terrestrial Networks Lab, Department of Systems and Computer Engineering, Carleton University, Ottawa, ON K1S 5B6, Canada

[2] Department of Electrical Engineering, Assiut University, Assiut 71516, Egypt

[3] Department of Electrical Engineering, Polytechnique Montreal, Montreal, QC H3T 1J4, Canada

[4] Department of Systems and Computer Engineering, Carleton University, Ottawa, ON K1S 5B6, Canada

[5] Digital Technologies Research Centre, National Research Council of Canada, Ottawa, ON K1A 0R6, Canada

[6] Division of Satellite Systems, MDA Space, Sainte-Anne-de-Bellevue, QC H9X 3R2, Canada

CORRESPONDING AUTHOR: M. ABDELSADEK (e-mail: mohammedabdelsadek@sce.carleton.ca)

This work was supported in part by the High Throughput and Secure Networks Challenge Program (CSTIP) at the National Research Council of Canada under Grant CH-HTSN-625; in part by MDA; and in part by Mitacs.

ABSTRACT Significant efforts are being made to integrate satellite and terrestrial networks into a unified wireless network. One major aspect of such an integration is the use of unified user terminals (UTs), which work for both networks and can switch seamlessly between them. However, supporting broadband connectivity for handheld UTs directly from low Earth orbit (LEO) satellite networks is very challenging due to link budget reasons. This paper proposes using distributed massive multiple-input multiple-output (DM-MIMO) techniques to improve the data rates of handheld devices with a view to supporting their broadband connectivity by exploiting the ultra-dense deployment of LEO satellites and high-speed inter-satellite links. In this regard, we discuss DM-MIMO-based satellite networks from different perspectives, including the channel model, network management, and architecture. In addition, we evaluate the performance of such networks theoretically by deriving closed-form expressions for spectral efficiency and using extensive simulations based on actual data from a Starlink constellation. The performance is compared with that of collocated massive MIMO connectivity (CMMC) and single-satellite connectivity (SSC) scenarios. The simulation results validate the analytical results and show the superior performance of DM-MIMO-based techniques compared to CMMC and SSC modes for improving the data rates of individual users.

INDEX TERMS Satellite communication networks, LEO constellations, distributed massive MIMO, direct satellite connectivity.

I. INTRODUCTION

THE INTEGRATION of satellite and terrestrial networks has received significant attention from standardization bodies, mobile network operators, satellite industries, and the research community, all of whom are interested in developing a unified wireless network. In this context, satellites are targeted to be part of both access and transport networks in a framework called non-terrestrial networks (NTNs), which is being standardized by the 3rd Generation Partnership Program (3GPP) [1]. The 3GPP aims to evolve the fifth-generation (5G) core network (5GC) and radio access network (RAN) to support NTNs. In this respect, the 3GPP has started studying the support of NTNs in 5G new radio (NR) in Release 15 [2]. In Releases 16 and 17,

several study and work items were implemented to investigate the support of NTNs in NR from different perspectives, including use cases and satellite access [3], management and orchestration with integrated satellite components [4], architecture [5], and solutions to enable such support [6]. Moreover, NTN is among the work items planned for Release 18 [7] and is expected to be one of the key pillars of the sixth-generation (6G) systems [8].

Despite that NTNs incorporate satellites at the geostationary orbit (GEO), medium Earth orbit (MEO), and low Earth orbit (LEO), LEO satellite networks have attracted more attention due to the recent developments in the satellite industry and their advantageous features. Several satellite companies (e.g., SpaceX, Telesat, Amazon, and OneWeb) have started (or announced their plans) to deploy thousands of LEO satellites by 2030, exploiting the advances in the small-size satellites industry that reduced their manufacturing and launching costs. This is considered one of the main game changers in satellite communications due to the advantages of LEO satellite networks compared to traditional GEOs. First, due to lower altitudes (e.g., 500 km compared to 36,000 km for GEOs), LEO satellite communications are characterized by their lower latency (e.g., 7.9 ms compared to 135 ms for GEOs) and lower propagation losses. This is in addition to their ultra-dense deployment and interconnection using high speed inter-satellite links (ISLs). This paves the way for a real integration between satellite and terrestrial networks in a unified space-terrestrial network as discussed in [9].

While the integration of satellite and terrestrial networks will be valuable for many applications, direct connectivity for handheld devices is considered a major targeted use case. This is because one key aspect of the harmonized operation between terrestrial and non-terrestrial networks is the use of a unified user terminal (UT) that works for both networks and that can seamlessly switch between them. Such a unified UT can enable use cases such as offloading, load balancing, and resilient network applications, to name a few [10]. In addition, direct connectivity for handheld devices (including unmodified smartphones) makes a compelling business case for satellite operators due to the large customer pool for this service compared to that for Very Small Aperture Terminals (VSATs). Moreover, this extends advanced 5G/6G services across the globe without the need for additional terrestrial infrastructure.

Support for handheld devices began with satellite phones that used large antennas for voice communications [11]. There have also been several demonstrations for supporting short messaging service (SMS) for unmodified smartphones in satellite networks [12]. However, supporting broadband services for unmodified handheld devices is particularly challenging due to link budget issues, even when using LEO satellites at low altitudes. One of the major technologies used to enable broadband connectivity in terrestrial networks is multiple-input multiple-output (MIMO) and its advanced versions (e.g., massive MIMO [13]), which are used to send multiple streams to the same user to increase the data rate. To tackle the link budget issue in satellite networks, a potential technology could be MIMO. Indeed, MIMO techniques have been studied for satellite communications from different perspectives and for different goals, as discussed below.

A. RELATED WORK

Several works have studied MIMO techniques for GEO satellite communications [14], [15], [16], [17], [18]. The authors in [14], for instance, adopted a multi-user MIMO model for GEO satellites serving a set of airplanes. In this context, the authors investigated the architecture required for spacecraft and satellite antenna design to achieve a multi-user MIMO gain in aviation networks. In [15], the authors studied the application of MIMO technology in both the feeder and user links of GEO satellites. The authors in [18] investigated the use of MIMO in GEO satellite broadcasting applications using dual polarization as an alternative to spatial MIMO with two satellites or two antennas on the same satellite. However, the focus of these studies was on the connectivity of ground user terminals (generally VSATs) to two GEO satellites (or a single satellite with two antennas) as a diversity technique to overcome fading due to adverse weather conditions. For the case of a multi-satellite connection, two GEO satellites were considered due to practical reasons (a small number of GEO satellites per operator are deployed since each satellite can cover a large portion of the Earth). Moreover, due to the long distances between the Earth and GEOs and the dominant line-of-sight (LoS) component, large antenna spacing (i.e., the distance between ground terminals) is required to achieve the multi-user MIMO gain as discussed in [14] and [19].

Exploiting the lower altitude of LEO satellites, a collocated massive MIMO technique was recently studied to improve the spectral efficiency of LEO satellite communications. The authors in [20], [21], [22] studied the application of massive MIMO in LEO satellite networks via deploying uniform planar arrays of antennas on LEO satellites to serve ground UTs. Along similar lines, in [23], the authors investigated the design of a beamforming codebook of massive MIMO-based LEO satellite communications compatible with 5G NR adopting a hybrid beamforming architecture. In this regard, they derived the associated footprint of an LEO satellite and designed the beamforming codebook such that the footprint would be covered by the beams in the codebook. The precoding design was studied for the case of hybrid analog/digital precoding in massive MIMO-based LEO satellite networks in [24] to maximize the energy efficiency using the alternating minimization and inexact majorization-minimization algorithms. The authors in [25] focus on the physical layer security aspect of satellites equipped with massive antenna systems in satellite-unmanned aerial vehicles (UAV) integrated networks.

However, as proven theoretically in [15] and experimentally in [19], to achieve a MIMO gain in satellite communications, it is required that either the satellites be

at different locations (to separate the satellite antennas properly), or the ground antenna elements be separated by a sufficient distance (in kilometers) to realize favourable channel conditions and avoid what is called keyhole channel capacity [15]. This means that the use of collocated massive MIMO techniques in LEO satellite networks may be used for multi-user MIMO transmissions, but this may not be efficient for single-user MIMO (i.e., sending multiple streams to the same user). That is, collocated massive MIMO may not be the right technology to help support broadband connectivity of handheld devices. Accordingly, the authors in [26] considered the joint transmission of two LEO satellites to a user terminal with multiple antennas and analyzed the outage probability. However, this work simply extended the basic MIMO model of GEO satellite communications to two LEO satellites without exploiting the capabilities of new LEO satellite constellations to significantly improve the throughput.

The ultra-dense deployment of LEO satellites and interconnection via high-speed, reliable, low-latency ISLs represents an unprecedented opportunity to utilize more advanced MIMO techniques such as cell-free massive MIMO (CF-mMIMO). This technology [27] was recently proposed for terrestrial networks, which builds on network MIMO, distributed antenna systems, coordinated multi-point (CoMP) joint transmission, and cloud radio access network (RAN) concepts. In this technology, the user is connected to a set of distributed access points that are connected to a central processing unit (CPU) to coordinate their cooperative transmission. CF-mMIMO shows great potential to substantially improve network performance (e.g., spectral efficiency and power efficiency) [28]. Utilizing this technology, our previous work in [29], [30] proposed a distributed massive MIMO (DM-MIMO)-based LEO satellite architecture exploiting the opportunities in the new LEO satellite constellations. This architecture could be used to support broadband connectivity for unmodified handheld devices in LEO satellite networks. In this paper, we investigate the use of DM-MIMO technology for this purpose and compare it with the collocated massive MIMO and classical single-input single-output (SISO) scenarios.

B. CONTRIBUTIONS AND STRUCTURE OF THE PAPER

The major contributions of this work can be summarized as follows:

- We propose a DM-MIMO-based LEO satellite network architecture that efficiently utilizes the multiple antennas at handheld devices to improve their data rates. This is achieved by exploiting distributed antenna systems in space that compensates for the collocation of UT antennas and forms the favourable channel conditions that are required to achieve massive MIMO gains.
- We establish a DM-MIMO channel model drawing on the 3GPP's studies and demonstrations. In so doing, we adopt Rician fading with random phase for the LoS component to accurately characterize the dynamics of the LEO satellite networks. In addition, we use standardized localization and satellite positioning systems for practical considerations.
- We study three satellite connectivity scenarios (i.e., DM-MIMO connectivity (DMMC), collocated massive MIMO connectivity (CMMC), and single-satellite connectivity (SSC)) and analyze their performances theoretically to show the superior performance of DMMC in comparison to traditional scenarios. In the process, we investigate the different aspects of network management (e.g., channel estimation, precoding, and downlink data transmission) and derive closed-form expressions for spectral efficiency. To the best of our knowledge, this is the first work that derives closed-form expressions for the spectral efficiency for multi-antenna users and satellites based on this channel model in satellite networks.
- We conduct extensive simulations based on actual data of the Starlink LEO satellite constellation and use practical system parameters from 3GPP reports. Drawing on this simulation, we evaluate the performance of DM-MIMO-based LEO satellite networks and compare them with CMMC and SSC scenarios from the perspective of spectral efficiency. In addition, we validate the analytical results through simulations. The experiments show a close match between theoretical and simulation results. The experiments also highlight the superior performance of DMMC compared to CMMC and SSC, which supports the potential of DM-MIMO technology to contribute to broadband connectivity for unmodified handheld devices via LEO satellite networks.

The remainder of the paper is organized as follows. Section II presents the network and channel models adopted in this study. In Section III, we analyze the three connectivity scenarios in detail and derive the corresponding spectral efficiency. In Section V, we discuss the details of the three connectivity scenario simulations and their performance evaluation and comparison. Finally, Section VI concludes the paper.

Notations: Throughout the paper, a lower case bold letter (e.g., $\mathbf{x}$) represents a vector. An upper case bold letter (e.g., $\mathbf{X}$) represents a matrix. The superscript $(\cdot)^H$ is the conjugate transpose of a matrix, and $(\cdot)^{-1}$ is its inverse. The function $\mathrm{tr}(\cdot)$ is the trace of the argument matrix. $\mathbb{E}\{\cdot\}$ is the expectation of the argument. The frequently used symbols are summarized in Table 1.

II. SYSTEM MODEL

A. NETWORK MODEL

We consider the downlink (DL) of an LEO satellite network composed of M satellites (SATs) indexed by $\mathcal{M} = \{1, 2, \ldots, m, \ldots, M\}$, in the visibility of a set of K UTs indexed by $\mathcal{K} = \{1, 2, \ldots, k, \ldots, K\}$. This set of UTs is uniformly distributed over the area under consideration and could be at ground-level or in the air.

TABLE 1. Frequently used symbols.

Symbol	Description
$\mathcal{K},\ \mathcal{M}$	Sets of UTs and SATs
$K,\ M$	Cardinalities of $\mathcal{K}$ and $\mathcal{M}$
$\mathcal{C}_k$	Set of UTs using the same pilot as UT k
$A,\ N$	Number of antennas per satellite and UT
$\tau_c,\ \tau_p$	Length of coherence interval and UL pilot
$L_{m,k}$	Large-scale fading coefficient (UT k–SAT m)
$\beta_{m,k},\ \lambda_{m,k}$	Large-scale parameters for LoS and NLoS components
$q_k,\ p_{m,k}$	Pilot power and DL power factor
$\phi_{m,k}$	Phase of LoS component
Ψ_k	Transmitted pilot signal of UT k
$h_{m,k}$	Channel coefficient between UT k and SAT m
$\mathbf{H}_{m,k}$	Channel matrix between UT k and SAT m
$\hat{\mathbf{H}}_{m,k}$	Estimated channel matrix between UT k and SAP m
$\mathbf{V}_{m,k}$	Precoding matrix for UT k and SAT m

To localize the UTs, we use a geodetic coordinate system (WGS 84 is the reference ellipsoid, which is the standard for the Global Positioning System (GPS)). Therefore, the position of the kth UT is determined by the tuple $(\text{Lat}_k, \text{Lon}_k, \text{Height}_k)$ to represent its latitude ($[-90°, 90°]$), longitude ($[-180°, 180°]$), and height (in meters), respectively.

To define the orbits of the satellites, we use Keplerian elements (orbital elements), which are composed of six parameters: the eccentricity and semimajor axis to determine the shape and size of the ellipsoid of the orbit; the inclination and right ascension of ascending node (RAAN) to define the orientation of the orbital plane in which the ellipsoid is embedded; the argument of periapsis (AoP); and the true anomaly (TA). These elements can be determined from the two line element (TLE) files of satellites that are accessible by the public.

To determine the satellite's position relative to a UT, we use the azimuth-elevation-range (AER) coordinate system. That is, the position of the mth SAT relative to the kth UT is expressed by the tuple $(\Omega_{m,k}, \theta_{m,k}, d_{m,k})$ to represent the azimuth, elevation, and range, respectively.

B. CHANNEL MODEL

a) Large-Scale Fading: To calculate the large-scale fading between UT k and SAT m, we use the following expression:

$$L_{m,k} = 10^{-\left(L^{\text{prop}}_{m,k}[\text{dB}]+L^{\text{shad}}_{m,k}[\text{dB}]+L^{\text{ant}}_{m,k}[\text{dB}]+L^{\text{other}}_{m,k}[\text{dB}]\right)/10}, \quad (1)$$

where:

- $L^{\text{prop}}_{m,k}[\text{dB}]$ is the path loss, which accounts for the free space propagation and can be calculated as [2]

$$L^{\text{prop}}_{m,k}[\text{dB}] = 32.45 + 20\log_{10} f_c + 20\log_{10} d_{m,k}, \quad (2)$$

  where f_c is the carrier frequency (in GHz) and $d_{m,k}$ is the separation distance (in meters).
- $L^{\text{shad}}_{m,k}[\text{dB}]$ represents the shadowing losses, which are modelled as a log-normal random variable (RV), i.e., $L^{\text{shad}}_{m,k}[\text{dB}] \sim \mathcal{N}(0, \sigma^2_{sh})$, where σ^2_{sh} is the shadowing variance.
- $L^{\text{ant}}_{m,k}[\text{dB}]$ represents the antenna gain losses due to the angle of the UT relative to the bore sight angle of the satellite's main antenna beam. This can be calculated as in the 3GPP report in [2] as follows

$$L^{\text{ant}}_{m,k}[\text{dB}] = -10\log_{10}\left(4\left|\frac{J_1(2\pi\eta\sin\omega_{m,k})}{2\pi\eta\sin\omega_{m,k}}\right|^2\right), \quad (3)$$

  where η is the antenna's aperture radius in wavelengths, $J_1(\cdot)$ is the Bessel function of the first kind and first order, and $\omega_{m,k}$ is the angle off the bore sight.
- $L^{\text{other}}_{m,k}[\text{dB}]$ represents the other large-scale losses, such as atmospheric gasses attenuation, ionospheric or tropospheric (based on the spectrum band used) scintillation, and building entry, as in [2].

b) Small-Scale Fading: We assume that the channel conditions are static during a coherence time interval of τ_c samples (channel uses). That is, we adopt a flat fading (i.e., non-frequency selective) model for the small-scale fading. The channels between the satellites and UTs consist of LoS and non-LoS (NLoS) components, where the probability of an LoS increases with the increase of the elevation angle (i.e., maximum at 90° elevation), as evaluated in [2]. Therefore, we model the channel between the kth UT and mth SAT as Rician, and this can be calculated as follows:

$$h_{m,k} = \sqrt{L_{m,k}}\left(\sqrt{\frac{\kappa_{m,k}}{\kappa_{m,k}+1}}e^{j\phi_{m,k}} + \sqrt{\frac{1}{\kappa_{m,k}+1}}h'_{m,k}\right), \quad (4)$$

where the two terms represent the LoS and NLoS components, respectively, and $\kappa_{m,k}$ is the Rician K-factor, which is the ratio of the LoS to NLoS powers. We suppose that the NLoS component is Rayleigh fading, i.e., $h'_{m,k} \sim \mathcal{CN}(0, 1)$, and the phase of the LoS component is $\phi_{m,k}$, which is a uniform random variable, i.e., $\phi_{m,k} \sim \mathcal{U}[-\pi, \pi]$. Due to the relative mobility between the satellites and UTs, we assume that the Doppler shift is compensated for in the synchronization process.

For simplicity, we rewrite (4) as follows:

$$h_{m,k} = \sqrt{\beta_{m,k}}e^{j\phi_{m,k}} + \sqrt{\lambda_{m,k}}h'_{m,k}, \quad (5)$$

where

$$\beta_{m,k} = \frac{\kappa_{m,k}}{\kappa_{m,k}+1}L_{m,k}, \quad (6)$$

$$\lambda_{m,k} = L_{m,k}/(\kappa_{m,k}+1). \quad (7)$$

Therefore, the large-scale parameters $\beta_{m,k}$ and $\lambda_{m,k}$ in (5) change slowly and can be known a priori.

III. CONNECTIVITY SCENARIOS

A. DM-MIMO-BASED CONNECTIVITY (DMMC)

In this connectivity scenario, we assume that the satellites are grouped into clusters of satellite access points (SAPs) which are connected to a CPU that is deployed on a super

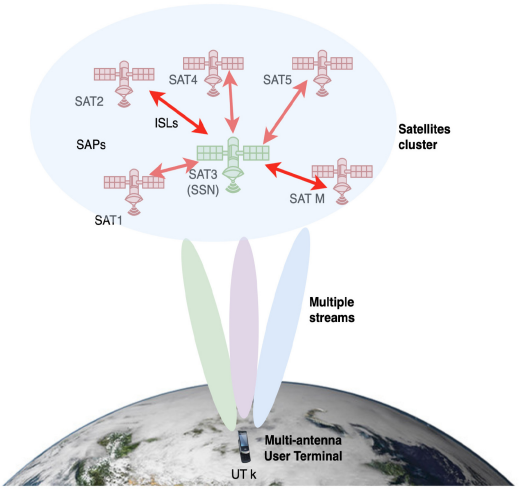

FIGURE 1. DMMC scenario.

satellite node (SSN) and controls the cooperative transmission of the SAPs to UTs, acting as a DM-MIMO system, as abstracted in Fig. 1. In addition, SSNs coordinate to handover UTs between clusters to keep the connectivitng of UTs to the network with minimal service interruptions. The concept of cluster handover in DM-MIMO-based LEO satellite networks is discussed in [29], [30]. We suppose that the transmission protocol is time division duplexing (TDD). That is, the coherence time interval is divided into three intervals: the initial τ_p samples are used for uplink (UL) pilot transmission, the subsequent τ_u samples are used for UL data transmission, and the last τ_d samples are reserved for DL data transmission. Therefore, the UL channel is estimated on the basis of the UL pilots and used to precode the DL data transmissions because this channel estimation is valid for the DL direction as well by virtue of channel reciprocity.

We assume that the UTs and SATs are equipped with A and N antennas, respectively. Therefore, the channel response matrix between the kth UT and mth SAP is $\mathbf{H}_{m,k} \in \mathbb{C}^{A\times N}$, and is given by

$$\mathbf{H}_{m,k} = \sqrt{\beta_{m,k}}e^{j\phi_{m,k}} + \sqrt{\lambda_{m,k}}\mathbf{H}'_{m,k}, \tag{8}$$

where $\mathbf{H}'_{m,k} \in \mathbb{C}^{A\times N}$ with elements that are i.i.d. circularly symmetric complex Gaussian random variables (RVs) with zero mean and unity variance. In this model, the LoS components of the received signals at different antennas are assumed to be the same due to the long distance between the satellite and UT relative to the separation distance between the antennas.

a) Channel Estimation: The UL channel is estimated at the SAPs utilizing the UL pilots. We assume that the pilots used for the N antennas of each UT are orthogonal. However, this set of pilots can be reused for other UTs, which yields pilot contamination. We denote the subset of UTs that use the same set of pilots as UT k as $\mathcal{C}_k$. The transmitted pilot signal from UT k is $\sqrt{q_k}\Psi_k \in \mathbb{C}^{\tau_p\times N}$, where q_k is the pilot power of UT k and $\Psi_k^H\Psi_k = \tau_p\mathbf{I}_N$, and $\mathbf{I}_N$ is the identity matrix of size N.

The signal received at the mth SAP from all UTs can be calculated as

$$\mathbf{Y}_m^P = \sum_{k=1}^{K}\sqrt{q_k}\mathbf{H}_{m,k}\Psi_k^H + \mathbf{W}_m^p, \tag{9}$$

where $\mathbf{Y}_m^P \in \mathbb{C}^{A\times\tau_p}$ represents the received pilot signals at the A-antennas of the mth SAP and $\mathbf{W}_m^p \in \mathbb{C}^{A\times\tau_p}$ represents the additive white Gaussian noise (AWGN) matrix with i.i.d. RVs elements that are complex Gaussian with zero mean and σ_{wp}^2 variance.

To estimate the UL channel of the kth UT, sufficient statistics are derived from the received signal as follows:

$$\mathbf{Y}_{m,k}^P = \mathbf{Y}_m^P\Psi_k = \sum_{i=1}^{K}\sqrt{q_i}\mathbf{H}_{m,i}\Psi_k^H\Psi_i + \mathbf{W}_m^p\Psi_k \tag{10}$$

$$= \sqrt{q_k}\tau_p\mathbf{H}_{m,k} + \sum_{k'\in\mathcal{C}_k\setminus\{k\}}\sqrt{q_{k'}}\tau_p\mathbf{H}_{m,k'} + \mathbf{W}_{m,k}^p. \tag{11}$$

This can be derived given that

$$\Psi_k^H\Psi_{k'} = \begin{cases}\tau_p\mathbf{I}_N, & k'\in\mathcal{C}_k\\ 0, & \text{otherwise.}\end{cases} \tag{12}$$

That is, there is pilot contamination resulting from the UTs using the same pilot set as UT k. From this statistic, the UL channel can be estimated using techniques such as minimum mean square error (MMSE) and least squares estimators [31], or by utilizing machine learning algorithms as in [32]. Without loss of generality, we use a phase-aware MMSE estimation in this paper. The MMSE estimate of the channel response can be derived as in Lemma 1.

Lemma 1: The phase-aware MMSE estimate of the channel response, $\mathbf{H}_{m,k}$, is given as:

$$\hat{\mathbf{H}}_{m,k} = \sqrt{\beta_{m,k}}e^{j\phi_{m,k}} + \lambda_{m,k}\sqrt{q_k}\tau_p\left(\mathbf{Y}_{m,k}^P - \sum_{i\in\mathcal{C}_k}\sqrt{q_i}\tau_p\sqrt{\beta_{m,i}}e^{j\phi_{m,i}}\right)\mathbf{A}_{m,k}, \tag{13}$$

where

$$\mathbf{A}_{m,k} = \left(\sum_{i\in\mathcal{C}_k}q_i\tau_p^2\lambda_{m,i}\mathbf{I}_N + \sigma_{wp}^2\mathbf{I}_N\right)^{-1}. \tag{14}$$

The error covariance matrix is given by:

$$\mathbf{C}_e = \mathbb{E}\left\{\left(\mathbf{H}_{m,k} - \hat{\mathbf{H}}_{m,k}\right)^H\left(\mathbf{H}_{m,k} - \hat{\mathbf{H}}_{m,k}\right)\right\}$$
$$= A\lambda_{m,k} - A\lambda_{m,k}^2 q_k\tau_p^2\mathbf{A}_{m,k}. \tag{15}$$

Proof: The proof is given in Appendix A. ■

b) DL Data Transmission: In the DL direction, the SAPs cooperatively transmit the data to the UTs. That is, the same symbol is transmitted to the UTs by the serving SAPs. We assume that the symbol to be sent to the kth UT is $\mathbf{s}_k \in \mathbb{C}^{N\times 1}$, where each element is a complex Gaussian RV with zero mean and unity variance and $\mathbb{E}\{\mathbf{s}_m\mathbf{s}_m^H\} = \mathbf{I}_N$. Each symbol is

precoded using the matrix $\mathbf{V}_{m,k} \in \mathbb{C}^{A\times N}$. For instance, for conjugate beamforming (CB), the precoding matrix of the mth SAP to the kth UT is

$$\mathbf{V}_{m,k} = \sqrt{p_{m,k}}\hat{\mathbf{H}}_{m,k}, \tag{16}$$

where $p_{m,k}$ is a power scaling factor and $\hat{\mathbf{H}}_{m,k}$ is the estimated UL/DL channel. Therefore, the transmitted signal from the mth SAP to all UTs, $\mathbf{x}_m \in \mathbb{C}^{A\times 1}$, is given by

$$\mathbf{x}_m = \sum_{k=1}^{K} \mathbf{V}_{m,k}\mathbf{s}_k. \tag{17}$$

Accordingly, the received signal at the kth UT is calculated by

$$\mathbf{y}_k = \sum_{m=1}^{M} \mathbf{H}_{m,k}^H \mathbf{x}_m + \mathbf{w}_k^d \tag{18}$$

$$= \sum_{m=1}^{M} \mathbf{H}_{m,k}^H \sum_{i=1}^{K} \mathbf{V}_{m,i}\mathbf{s}_i + \mathbf{w}_k^d \tag{19}$$

$$= \sum_{m=1}^{M}\sum_{i=1}^{K} \mathbf{H}_{m,k}^H \mathbf{V}_{m,i}\mathbf{s}_i + \mathbf{w}_k^d \tag{20}$$

$$= \sum_{i=1}^{K} \mathbf{D}_{k,i}\mathbf{s}_i + \mathbf{w}_k^d, \tag{21}$$

where $\mathbf{w}_k^d \in \mathbb{C}^{N\times 1}$ is the AWGN vector at the kth UT and $\mathbf{D}_{k,i} = \sum_{m=1}^{M} \mathbf{H}_{m,k}^H \mathbf{V}_{m,i}$ is the precoded channel from all SAPs. Since the UT does not know the precoded channel gain a priori, it approximates it either with the mean value (statistical channel state information), $\mathbb{E}\{\mathbf{D}_{k,k}\}$, or estimates it. In this paper, we assume that the UT uses the mean value, which is adopted in several studies in the literature (e.g., [27], [33]). Therefore, the received signal can be written in the following form:

$$\mathbf{y}_k = \mathbb{E}\{\mathbf{D}_{k,k}\}\mathbf{s}_k + \left(\mathbf{D}_{k,k} - \mathbb{E}\{\mathbf{D}_{k,k}\}\right)\mathbf{s}_k + \sum_{i=1,i\neq k}^{K} \mathbf{D}_{k,i}\mathbf{s}_i + \mathbf{w}_k^d, \tag{22}$$

where these components are the desired, unknown, interference, and noise, respectively. Therefore, the spectral efficiency of the kth UT in this DMMC scenario is

$$R_k^{\text{DMMC}} = \frac{\tau_c - \tau_p}{\tau_c}\log_2\left(\left|\mathbf{I}_N + \text{SINR}_k^{\text{DMMC}}\right|\right), \tag{23}$$

where

$$\text{SINR}_k^{\text{DMMC}} = \mathbf{G}_k^H \mathbf{B}_k^{-1}\mathbf{G}_k, \tag{24}$$

$$\mathbf{G}_k = \mathbb{E}\{\mathbf{D}_{k,k}\} = \mathbb{E}\left\{\sum_{m=1}^{M} \mathbf{H}_{m,k}^H \mathbf{V}_{m,k}\right\}, \tag{25}$$

$$\mathbf{B}_k = \mathbb{E}\left\{\sum_{m=1}^{M}\sum_{n=1}^{M}\sum_{i=1}^{K} \mathbf{H}_{m,k}^H \mathbf{V}_{m,i}\mathbf{V}_{n,i}^H \mathbf{H}_{n,k}\right\} - \mathbf{G}_k\mathbf{G}_k^H + \sigma_{w_k^d}^2\mathbf{I}_N. \tag{26}$$

For conjugate beamforming, this signal to noise and interference ratio (SINR) can be calculated as in Theorem 1.

Theorem 1: For conjugate beamforming (i.e., $\mathbf{V}_{m,k}$ is given as in (16)), $\mathbf{G}_k$ and $\mathbf{B}_k$ are calculated as follows:

$$\mathbf{G}_k = \sum_{m=1}^{M} A\sqrt{p_{m,k}}\left(\beta_{m,k} + \lambda_{m,k}^2\tau_p^2 q_k \mathbf{A}_{m,k}\right), \tag{27}$$

$$\mathbf{B}_k = \mathcal{T}_1 + \mathcal{T}_2 - \mathbf{G}_k\mathbf{G}_k^H + \sigma_{w_k^d}^2\mathbf{I}_N, \tag{28}$$

where $\mathcal{T}_1$ and $\mathcal{T}_2$ are given in (29) and (30), respectively, shown at the bottom of the page.

Proof: The proof is given in Appendix B. ■

B. CM-MIMO-BASED CONNECTIVITY (CMMC)

In this connectivity scenario, a single satellite replaces the cluster of satellites serving the UTs, as depicted in Fig. 2. However, this single satellite is equipped with $A' = MA$ antennas and transmits $MP^{\max}$ maximum power, where $P^{\max}$ is the maximum power per satellite in the DMMC scenario. In addition, the TDD frame, UL pilot transmission, and DL data precoding are the same as in the DMMC mode. Therefore, this structure is equivalent to the DMMC scenario but with the antennas collocated at a single satellite.

$$\mathcal{T}_1 = \sum_{m=1}^{M}\sum_{i=1}^{K} p_{m,i}A^2 N\beta_{m,k} + p_{m,i}\lambda_{m,k}^3 q_k\tau_p^2 \times \begin{cases} \left(3\tau_p^2 q_k\lambda_{m,k} + \sum_{\substack{k'\in\mathcal{C}_i\\ k'\neq k}} \tau_p^2 q_{k'}\lambda_{m,k'} + \sigma_{w^p}^2\right) AN\text{tr}\left(\mathbf{A}_{m,i}\mathbf{A}_{m,i}^H\right)\mathbf{A}_{m,i}^{-1}, & k\in\mathcal{C}_i \\ AN\text{tr}\left(\mathbf{A}_{m,i}\mathbf{A}_{m,i}^H\right)\mathbf{A}_{m,i}^{-1}, & k\notin\mathcal{C}_i \end{cases} \tag{29}$$

$$\mathcal{T}_2 = \sum_{m=1}^{M}\sum_{\substack{n=1\\ n\neq m}}^{M}\sum_{i=1}^{K} \sqrt{p_{m,i}p_{n,i}}A^2 N\sqrt{\beta_{m,k}\beta_{m,i}\beta_{n,i}\beta_{n,k}}e^{-j\phi_{m,k}}e^{j\phi_{m,i}}e^{-j\phi_{n,i}}e^{j\phi_{n,k}}\mathbf{1}_N + \begin{cases} \sqrt{p_{m,i}p_{n,i}}\lambda_{m,k}\lambda_{m,i}\lambda_{n,i}\lambda_{n,k}q_i^2\tau_p^4 A^2\mathbf{A}_{m,i}\mathbf{A}_{n,i}^H, & k\in\mathcal{C}_i \\ 0, & k\notin\mathcal{C}_i \end{cases} \tag{30}$$

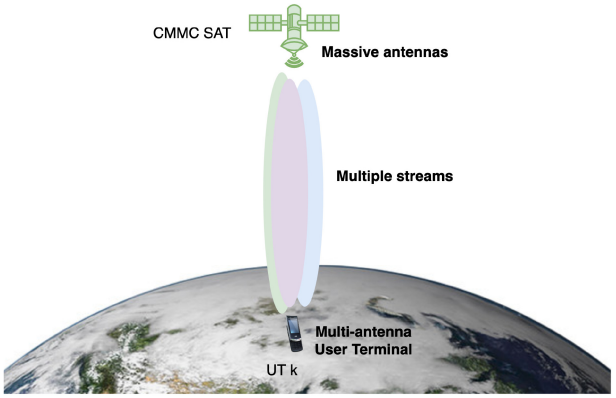

FIGURE 2. CMMC scenario.

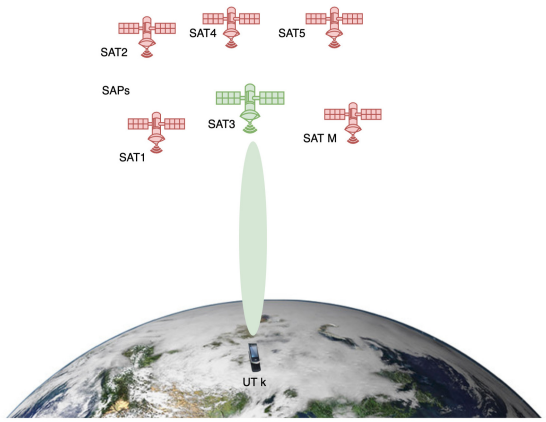

FIGURE 3. SSC scenario.

The analysis of the channel estimation and DL data transmission investigated in Section III-A is valid here by inserting $M = 1$ and $A = A'$ in the expressions. Therefore, the spectral efficiency of UT k is expressed as follows:

$$R_k^{\text{CMMC}} = \frac{\tau_c - \tau_p}{\tau_c} \log_2\left(\left|\mathbf{I}_N + \text{SINR}_k^{\text{CMMC}}\right|\right), \tag{31}$$

where

$$\text{SINR}_k^{\text{CMMC}} = \tilde{\mathbf{G}}_k^H \tilde{\mathbf{B}}_k^{-1} \tilde{\mathbf{G}}_k, \tag{32}$$

$$\tilde{\mathbf{G}}_k = \mathbb{E}\left\{\mathbf{H}_{m^*,k}^H \mathbf{V}_{m^*,k}\right\}, \tag{33}$$

$$\tilde{\mathbf{B}}_k = \mathbb{E}\left\{\sum_{i=1}^{K} \mathbf{H}_{m^*,k}^H \mathbf{V}_{m^*,i} \mathbf{V}_{m^*,i}^H \mathbf{H}_{m^*,k}\right\} - \tilde{\mathbf{G}}_k \tilde{\mathbf{G}}_k^H + \sigma_{w_k^d}^2 \mathbf{I}_N, \tag{34}$$

where $\mathbf{H}_{m^*,k} \in \mathbb{C}^{A' \times N}$ and $\mathbf{V}_{m^*,k} \in \mathbb{C}^{A' \times N}$ are the channel response and precoding matrices between UT k and the CMMC satellite, m^*, respectively.

Lemma 2: For conjugate beamforming (i.e., $\mathbf{V}_{m^*,k}$ is given as in (16)), $\tilde{\mathbf{G}}_k$ is calculated as follows:

$$\tilde{\mathbf{G}}_k = A' \sqrt{p_{m^*,k}} \left(\beta_{m^*,k} + \lambda_{m^*,k}^2 \tau_p^2 q_k \mathbf{A}_{m^*,k}\right), \tag{35}$$

and $\tilde{\mathbf{B}}_k$ is given as in (36), shown at the bottom of the page.

Proof: The proof is similar to that of Theorem 1 after inserting $M = 1$ and replacing A by A'. ■

C. SINGLE SATELLITE CONNECTIVITY (SSC)

In this baseline connectivity scenario, the SISO mode is adopted. That is, each single-antenna UT is connected to a single satellite that is equipped with a single antenna, as shown in Fig. 3. The selection of the serving satellite is based on the channel coefficient. Therefore, every UT is connected to the SAT with the best channel coefficient. The spectral efficiency of UT k can be calculated as follows:

$$R_k^{\text{SSC}} = \frac{1}{F} \mathbb{E}\left\{\log_2\left(1 + \frac{p_{m',k}|h_{m',k}|^2}{\sigma_{w_k}^2}\right)\right\}, \tag{37}$$

where m' is the index of the SAT that transmits to UT k, $\sigma_{w_k}^2$ is the variance of the AWGN at the UT, $p_{m',k}$ is the power allocated to this UT, and F is the frequency reuse factor adopted in the system to address the co-channel interference, which reduces the spectrum resources available per spot.

IV. CHALLENGES OF DMMC AND POTENTIAL SOLUTIONS

In this section, we discuss the major challenges and open issues associated with implementing DMMC approach in LEO satellite networks and potential solutions.

A. OUTDATED CHANNEL INFORMATION

As we discussed in Section III-A, UL pilots can be utilized to estimate channel conditions and be used to design DL precoding matrices. However, due to the long propagation delay, this UL channel state information (CSI) may be outdated to be considered for DL channel conditions. There are several works in the literature that investigate this challenge in LEO

$$\tilde{\mathbf{B}}_k = \sum_{i=1}^{K} p_{m^*,i} A'^2 N \beta_{m^*,k} + p_{m^*,i} \lambda_{m^*,k}^3 q_k \tau_p^2 \times \begin{cases} \left(3\tau_p^2 q_k \lambda_{m^*,k} + \sum_{\substack{k' \in \mathcal{C}_i \\ k' \neq k}} \tau_p^2 q_{k'} \lambda_{m^*,k'} + \sigma_{w^p}^2\right) A' N \text{tr}\left(\mathbf{A}_{m^*,i} \mathbf{A}_{m^*,i}^H\right) \mathbf{A}_{m^*,i}^{-1}, & k \in \mathcal{C}_i \\ A' N \text{tr}\left(\mathbf{A}_{m^*,i} \mathbf{A}_{m^*,i}^H\right) \mathbf{A}_{m^*,i}^{-1}, & k \notin \mathcal{C}_i \end{cases} - \tilde{\mathbf{G}}_k \tilde{\mathbf{G}}_k^H + \sigma_{w_k^d}^2 \mathbf{I}_N \tag{36}$$

satellite networks. For instance, the authors in [32] propose exploiting the correlation of changing channels to address this channel aging issue. In this regard, a deep learning-based satellite channel predictor using long short term with memory (LSTM) units to predict future CSI in LEO satellite networks. The authors in [34] utilize a deep neural network (DNN) to deeply mine the potential correlation between uplink and downlink and predict downlink CSI. Therefore, utilizing such advanced techniques can tackle this issue.

B. SYNCHRONIZATION

The cooperative transmission of LEO satellites in the proposed approach requires synchronization among them. This synchronization is challenging due to the movement of the satellites. However, several techniques have been proposed in the literature to address this challenge. For example, the authors in [35] propose a two way time transfer (TWTT) based method to achieve time synchronization in distributed satellite systems. In addition, closed-loop and open-loop phase and frequency synchronization have been investigated in several studies [36], [37]. Such approaches can be utilized to achieve synchronization between satellites.

C. SIGNALLING OVERHEAD AND COMPUTATIONAL COMPLEXITY

As discussed in Section III-A, a cluster of SAPs is controlled by an SSN to cooperatively communicate with UTs. This centralized control and data processing requires additional computational resources at SSNs. Besides, exchanging control and data information between the SAPs and the SSN is needed, which entails signalling overhead. However, several techniques can be applied to alleviate these issues. First, the number of SSNs with advanced computing resources can be optimized to balance the cost and load per SSN. Second, this cooperative transmission should not be implemented for all served UTs. For example, a UT with low data rate requirements may be served by a single SAP, but a high throughput UT may be served by the most suitable SAPs subset without activating all cluster SAPs to serve such UTs. Serving UTs with a subset of cluster SAPs is the main idea of user-centric CF-mMIMO as discussed in [38]. This has been implicitly adopted in [30] by setting the power control coefficient of non-serving SAPs to zero. Moreover, the control signalling between SAPs and the SSN can be minimized by allowing some functions to be processed locally at SAPs, e.g., using conjugate beamforming techniques with locally-estimated channels and precoding matrices. Furthermore, free-space optical (FSO) technologies [39] can play a significant role in LEO satellite networks, which allow high-speed, reliable, and low-latency ISLs and could address fronthaul signalling overhead issues.

V. SIMULATION RESULTS

In this section, we evaluate the performance of an LEO satellite network serving a set of UTs under the three UT connectivity scenarios, we use MATLAB's Satellite Communications Toolbox. In doing so, we simulate each scenario and calculate the corresponding performance indicators. It is worth noting that the focus of this paper is to compare the proposed DM-MIMO-based satellite network approach with traditional connectivity scenarios from the perspective of broadband connectivity of handheld devices. For this purpose, the literature on multiple-antenna techniques that can be applied in a distributed or centralized manner is rich. Each technique has its advantages and disadvantages. For instance, conjugate beamforming may not provide the optimal performance of beamforming in multiple antenna systems. However, it can be implemented locally at the SAPs in a distributed manner without the need to forward the channel estimates to the CPU. On the other hand, there are several centralized beamforming techniques (e.g., minimum mean square error (MMSE)-based) that can be used to optimize the beamforming vectors to minimize the interference between the co-scheduled users and spatial layers. Nevertheless, additional signalling would be required to allow the CPU to collect the channel parameters from the SAPs and calculate the corresponding beamforming vectors. Therefore, without loss of generality, we adopt conjugate beamforming in this study as been widely used in cell-free massive MIMO literature (e.g., [27], [38]) to minimize the signalling overhead on fronthaul links. Similarly, we use the widely multiple-antenna techniques as representatives of the different approaches and focus on using the same technique for both the distributed and collocated scenarios to make the comparison fair and show the effectiveness of the distributed antenna approach.

We consider a set of UTs distributed uniformly over the area between latitudes 44° and 54° and longitudes −86° and −80°. This set of UTs is served using a group of LEO satellites. For this purpose, we utilize the Starlink LEO satellites that were visible to the set of UTs on May 1, 2022, at 15:45 UTC. The IDs and Keplerian elements of those satellites are given in Table 2. For the DMMC and SSC scenarios, the UTs are connected to these satellites as a cluster or single-satellites, respectively. For the CMMC mode, this set of satellites is replaced by an equivalent satellite (referred to as CMMC SAT) that is positioned at the location of the satellite with the closest distance to the UTs. The simulated satellite scenario is shown in Fig. 4.

Different realizations for the channel between the UTs and SATs are generated on the basis of the model discussed in Section II-B. The number of realizations and setups and link parameters are summarized in Table 3. These channel matrices are then estimated using phase-aware MMSE estimators as in Lemma 1.

Based on the channel estimates, the downlink precoding matrices are calculated as in (16) for the DMMC and CMMC scenarios. The power control coefficient is calculated as follows:

$$p_{m,k} = \frac{\beta_{m,k} + \lambda_{m,k}}{\mathbb{E}\left\{||\hat{\mathbf{H}}_{m,k}||^2\right\} \sum_{i=1}^{K} \beta_{m,i} + \lambda_{m,i}} P_m^{\max}, \qquad (38)$$

TABLE 2. Satellite scenario parameters.

Satellite	Semimajor Axis	Eccentricity	Inclination	RAAN	AoP
STARLINK-2653	6,925 km	1.560×10^{-4}	53.0514°	314.7596°	59.2361°
STARLINK-1377	6,925 km	1.292×10^{-4}	53.0547°	308.4176°	73.3720°
STARLINK-2094	6,925 km	1.604×10^{-4}	53.0525°	264.6603°	53.8621°
STARLINK-1395	6,925 km	1.652×10^{-4}	53.0539°	258.4343°	53.3828°
STARLINK-2512	6,925 km	1.432×10^{-4}	53.0552°	304.7527°	62.6049°
STARLINK-2547	6,925 km	1.390×10^{-4}	53.0531°	284.7672°	70.6251°
STARLINK-1544	6,925 km	1.661×10^{-4}	53.0544°	328.4255°	73.0011°
STARLINK-1344	6,925 km	1.496×10^{-4}	53.0529°	288.3541°	67.0844°
STARLINK-2717	6,925 km	1.492×10^{-4}	53.0542°	324.7078°	73.2488°
STARLINK-2649	6,925 km	1.522×10^{-4}	53.0549°	314.7545°	63.6051°
STARLINK-1454	6,925 km	1.607×10^{-4}	53.0538°	268.3902°	57.4986°

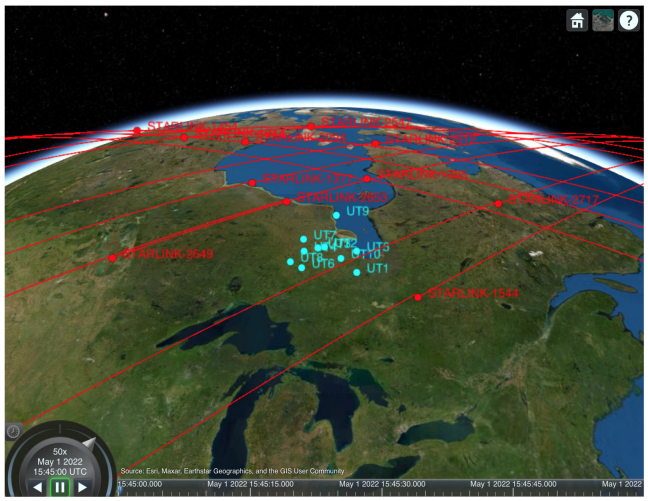

FIGURE 4. Simulated satellite scenario in MATLAB.

where $P_m^{\max}$ is the maximum transmit power of SAT m, and $\mathbb{E}\{||\hat{\mathbf{H}}_{m,k}||^2\}$ can be derived using (15) as $\mathbb{E}\{||\hat{\mathbf{H}}_{m,k}||^2\} = AN\beta_{m,k} + A\lambda_{m,k}^2 q_k \tau_p^2 \mathrm{tr}(\mathbf{A}_{m,k})$. That is, the power is allocated in proportion to the channel quality of the UT in the three scenarios of connectivity. For the SSC mode, the satellite-UT assignment is implemented on the basis of the best channel coefficient to maximize the data rate of the UTs. Finally, the achievable data rates are estimated using the expressions in (23), (31), and (37), for the DMMC, CMMC, and SSC modes, respectively.

Fig. 5 shows the spectral efficiency versus A. We should note that A represents the number of antennas at each satellite in the DMMC mode. However, for the CMMC mode, the total number of antennas is given by multiplying the number of antennas per satellite by the number of satellites used in the DMMC mode (i.e., $A' = MA$). This figure shows both the simulations and analytical results for the DMMC and CMMC modes, which reveals a close match between them and validates the analysis in Section III.

Fig. 6 shows the spectral efficiency versus A at different values of M for the three scenarios of connectivity. As we can see in the figure, deploying more antennas in the CMMC scenario does not substantially increase the gain. That is,

TABLE 3. Simulation parameters.

Parameter	Value
Carrier frequency	2 GHz (S-band) [2]
Antenna factor (η)	10 wavelengths [2]
Shadowing std	5 dB
Noise figure	7 dB [6]
Noise power spectral density	-174 dBm/Hz
Rician K-factor ($\kappa_{m,k}$)	10 dB
Satellite max. power ($P_m^{\max}$)	15 dBW
Satellite max. antenna gain	30 dBi [6]
UT antenna gain	0 dBi [6]
Pilot power (q_k)	0 dBW
Coherence intervals: τ_c, τ_p	300, 10 samples
Number of channel realizations	1000
Number of setups	30, 1000
Frequency reuse factor for SSC (F)	4

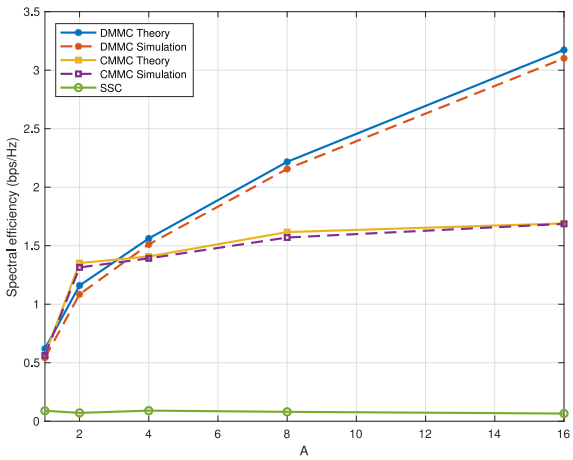

FIGURE 5. Spectral efficiency versus A using the three connectivity scenarios based on simulations and analytical results (i.e., for DMMC and CMMC) at $M = 4$ and $N = 4$.

the data rate improvement reaches saturation rapidly at a low number of antennas. However, deploying more antennas helps to improve the data rates even more in the DMMC scenario. In addition, the figure shows that the spectral efficiency based on the DMMC architecture increases with the increase of the number of SAPs (M) while achieving significantly

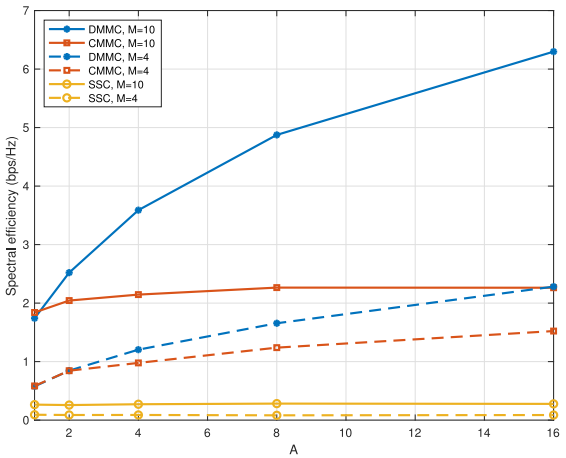

FIGURE 6. Average data rate per UT versus number of antennas per satellite (A) using the three connectivity scenarios at different values of M and $N = 2$.

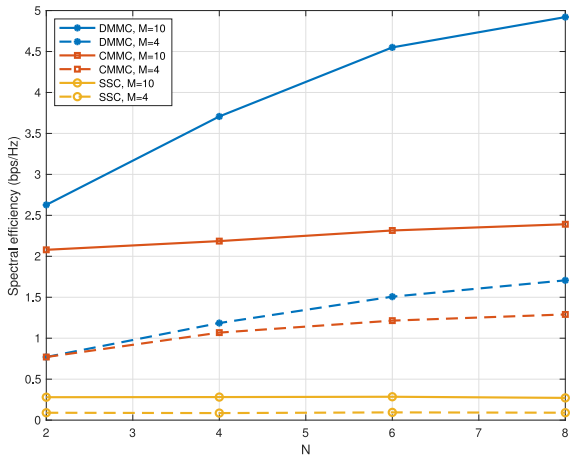

FIGURE 7. Spectral efficiency versus the number of antennas per UT (N) using the three connectivity scenarios at different values of M and $A = 2$.

higher rates in comparison to the CMMC and SSC scenarios. This is because of the macro-diversity and favorable channel conditions that are introduced by the distributed antenna deployment. Therefore, increasing the number of distributed antenna elements increases the gain. For the CMMC mode, the multiple antenna transmission achieves a certain gain in terms of data rates compared to the SSC scenario. However, this gain has a limit that depends on the spatial dimensions of the channel matrix. Therefore, increasing the number of antennas at the CMMC satellite (which is equivalent to increasing the number of SAPs in the DMMC scenario) does not help increase the rate beyond that limit (for the same UT). This low spatial dimensionality of the channel matrix results from the almost-identical channel paths from the different antennas at the UT to those at the satellite due to the long distance and dominant LoS component.

Fig. 7 shows the spectral efficiency versus the number of antennas at each UT (N) for the three connectivity scenarios at different values of M. Similar to increasing the number of antennas at the satellites, this slowly improves the data rates in the CMMC scenario. However, to a greater extent, this enhances the data rates in the DMMC mode. Again, increasing the number of satellites (M) increases the spectral efficiency in all scenarios. However, the DMMC mode shows significantly higher gain.

Accordingly, the results reveal that DMMC can be utilized to improve the data rate of users by exploiting a large number of visible satellites. This technique enables the network to utilize the spatial dimensions to send multiple streams to the same UT while compensating for the antenna separation requirement by using a distributed antenna system at the satellite network side. In doing so, the keyhole capacity that happens in collocated massive MIMO systems can be avoided.

VI. CONCLUSION

In this paper, we investigated the use of DM-MIMO technology in LEO satellite networks to improve the spectral efficiency of users with a view to supporting broadband connectivity for handheld devices. To this end, we studied a DM-MIMO-based satellite network from different perspectives, evaluated the performance theoretically and using simulations, and compared its performance with collocated massive MIMO and single-satellite connectivity scenarios. The results showed that the distributed antenna-based connectivity could be the right technique to achieve the desired gains of massive MIMO in LEO satellite networks, which would be similar to that experienced in terrestrial networks. The collocated antenna system can be used to multiplex the transmissions of different UTs that are sufficiently separated on the ground. However, this may not help to improve the data rate of a single UT that requires broadband connectivity. Nevertheless, the benefits of using DM-MIMO come at the cost of implementing a cooperative inter-satellite framework to serve the same set of UTs. This coordination will require additional inter-satellite signaling and processing.

As discussed in Section IV, there are several challenges and open issues to optimize DM-MIMO-based LEO satellite networks for broadband connectivity of handheld devices. As future work, we will investigate the impact of synchronization errors and channel information aging on achieving broadband connectivity for handheld devices. In addition, dynamic clustering will be studied to exclude some SAPs from serving certain users to save energy, reduce signalling overhead, and decrease computational complexity on SSBs. Moreover, different multiple-antenna techniques (e.g., other distributed and centralized beamforming approaches) will be investigated and evaluated.

APPENDIX A
PROOF OF LEMMA 1

Proof: The metric in (11) can be written in vector form as follows:

$$\mathrm{vec}\left(\mathbf{Y}^{P}_{m,k}\right) = \sqrt{q_k}\tau_p \mathbf{I}_{AN}\mathrm{vec}\left(\mathbf{H}_{m,k}\right) + \sum_{k' \in \mathcal{C}_k \setminus \{k\}} \sqrt{q_{k'}}\tau_p \mathrm{vec}\left(\mathbf{H}_{m,k'}\right) + \mathrm{vec}\left(\mathbf{W}^{p}_{m,k}\right), \tag{39}$$

where vec($\mathbf{X}$) is the vectorization of matrix $\mathbf{X}$ by stacking all the columns on top of each other.

As in [33, Lemma B.17], for a general vector $\mathbf{x} \in \mathbb{C}^{N\times 1} \sim \mathcal{CN}(\bar{\mathbf{x}}, \mathbf{C_x})$ can be estimated from an observation vector $\mathbf{y} \in \mathbb{C}^{L\times 1}$ in the following form:

$$\mathbf{y} = \mathbf{A}\mathbf{x} + \mathbf{n}, \tag{40}$$

where $\mathbf{A} \in \mathbb{C}^{L\times N}$ is a known matrix and $\mathbf{n} \in \mathbb{C}^{L\times 1} \sim \mathcal{CN}(\bar{\mathbf{n}}, \mathbf{C_n})$ is a noise/interference vector. The MMSE estimate of $\mathbf{x}$ is as follows:

$$\hat{\mathbf{x}}_{\text{MMSE}}(\mathbf{y}) = \bar{\mathbf{x}} + \mathbf{C_x}\mathbf{A}^H\left(\mathbf{A}\mathbf{C_x}\mathbf{A}^H + \mathbf{C_n}\right)^{-1}(\mathbf{y} - \mathbf{A}\bar{\mathbf{x}} - \bar{\mathbf{n}}). \tag{41}$$

Therefore, (39) can be rewritten in the form in (40) by assuming that $\mathbf{x} = \text{vec}(\mathbf{H}_{m,k})$, $\mathbf{A} = \sqrt{q_k}\tau_p\mathbf{I}_{AN}$, $\mathbf{y} = \text{vec}(\mathbf{Y}^P_{m,k})$, and $\mathbf{n} = \sum_{k'\in\mathcal{C}_k\setminus\{k\}}\sqrt{q_{k'}}\tau_p\text{vec}(\mathbf{H}_{m,k'}) + \text{vec}(\mathbf{W}^p_{m,k})$. Accordingly, the statistics of these parameters are given as:

$$\bar{\mathbf{x}} = \sqrt{\beta_{m,k}}e^{\phi_{m,k}}\mathbf{1}_{AN}, \tag{42}$$

$$\mathbf{C_x} = \lambda_{m,k}\mathbf{I}_{AN}, \tag{43}$$

$$\bar{\mathbf{n}} = \sum_{k'\in\mathcal{C}_k\setminus\{k\}}\sqrt{q_{k'}}\tau_p\sqrt{\beta_{m,k'}}e^{j\phi_{m,k'}}\mathbf{1}_{AN}, \tag{44}$$

$$\mathbf{C_n} = \sum_{k'\in\mathcal{C}_k\setminus\{k\}} q_{k'}\tau_p^2\sqrt{\lambda_{m,k'}}\mathbf{I}_{AN} + \sigma^2_{w^p}\mathbf{I}_{AN}, \tag{45}$$

where $\mathbf{1}_{AN}$ is the ones vector of length AN.

Accordingly, the estimated channel vector is calculated as in (46). This can be returned to matrix notation as in (13).

$$\begin{aligned}
\text{vec}\left(\hat{\mathbf{H}}_{m,k}\right) &= \sqrt{\beta_{m,k}}e^{j\phi_{m,k}}\mathbf{1}_{AN} + \lambda_{m,k}\sqrt{q_k}\tau_p\mathbf{I}_{AN} \\
&\left(q_k\tau_p^2\lambda_{m,k}\mathbf{I}_{AN} + \sigma^2_{w^p}\mathbf{I}_{AN} + \sum_{k'\in\mathcal{C}_k\setminus\{k\}} q_{k'}\tau_p^2\sqrt{\lambda_{m,k'}}\mathbf{I}_{AN}\right)^{-1} \\
&\times\left(\text{vec}\left(\mathbf{Y}^P_{m,k}\right) - \sqrt{q_k}\tau_p\sqrt{\beta_{m,k}}e^{j\phi_{m,k}}\mathbf{1}_{AN}\right. \\
&\left. - \sum_{k'\in\mathcal{C}_k\setminus\{k\}}\sqrt{q_{k'}}\tau_p\sqrt{\beta_{m,k'}}e^{j\phi_{m,k'}}\mathbf{1}_{AN}\right) \\
&= \sqrt{\beta_{m,k}}e^{j\phi_{m,k}}\mathbf{1}_{AN} + \lambda_{m,k}\sqrt{q_k}\tau_p\mathbf{I}_{AN} \\
&\left(\sum_{i\in\mathcal{C}_k} q_i\tau_p^2\sqrt{\lambda_{m,i}}\mathbf{I}_{AN} + \sigma^2_{w^p}\mathbf{I}_{AN}\right)^{-1} \\
&\times\left(\text{vec}\left(\mathbf{Y}^P_{m,k}\right) - \sum_{i\in\mathcal{C}_k}\sqrt{q_i}\tau_p\sqrt{\beta_{m,i}}e^{j\phi_{m,i}}\mathbf{1}_{AN}\right)
\end{aligned} \tag{46}$$

To prove (15), we use the covariance matrix of the MMSE estimation error, $\tilde{\mathbf{x}} = \mathbf{x} - \hat{\mathbf{x}}$, utilizing the general form in (40), which can be calculated as [33, Lemma B.17]

$$\mathbf{C}_{\tilde{\mathbf{x}}} = \mathbf{C_x} - \mathbf{C_x}\mathbf{A}^H\left(\mathbf{A}\mathbf{C_x}\mathbf{A}^H - \mathbf{C_n}\right)^{-1}\mathbf{A}\mathbf{C_x}. \tag{47}$$

Therefore, the covariance of the estimation error of the vector $\mathbf{x} = \text{vec}(\mathbf{H}_{m,k})$ can be calculated as follows:

$$\begin{aligned}
\mathbf{C}_{\tilde{\mathbf{x}}} &= \lambda_{m,k}\mathbf{I}_{AN} - \lambda_{m,k}q_k\tau_p\mathbf{I}_{AN} \\
&\cdot\left(\sum_{i\in\mathcal{C}_k} q_i\tau_p^2\sqrt{\lambda_{m,i}}\mathbf{I}_{AN} + \sigma^2_{w^p}\mathbf{I}_{AN}\right)^{-1}\cdot\lambda_{m,k}q_k\tau_p\mathbf{I}_{AN}
\end{aligned} \tag{48}$$

Accordingly, the expression in (15) is given by rewriting this $\mathbf{C}_{\tilde{\mathbf{x}}}$ into matrix form. ■

APPENDIX B
PROOF OF THEOREM 1

Proof: To simplify the derivation of (27) and (28), we rewrite $\hat{\mathbf{H}}_{m,k}$ and drop the commas in the subscripts. From (8), (11), and (13), $\hat{\mathbf{H}}_{m,k}$ can be written in the following form:

$$\begin{aligned}
\hat{\mathbf{H}}_{mk} &= \sqrt{\beta_{mk}}e^{j\phi_{mk}} + \lambda_{mk}\sqrt{q_k}\tau_p \\
&\left(\sum_{i\in\mathcal{C}_k}\sqrt{q_i}\tau_p\mathbf{H}_{mi} + \mathbf{W}^p_{mk} - \sum_{i\in\mathcal{C}_k}\sqrt{q_i}\tau_p\sqrt{\beta_{mi}}e^{j\phi_{mi}}\right)\mathbf{A}_{mk} \\
&= \sqrt{\beta_{mk}}e^{j\phi_{mk}} + \lambda_{mk}\sqrt{q_k}\tau_p\left(\sum_{i\in\mathcal{C}_k}\sqrt{q_i}\tau_p\sqrt{\lambda_{mi}}\mathbf{H}'_{mi} + \mathbf{W}^p_{mk}\right)\mathbf{A}_{mk}.
\end{aligned} \tag{49}$$

Then, $\mathbf{G}_{m,k}$ can be derived as follows:

$$\begin{aligned}
\mathbf{G}_k &= \mathbb{E}\left\{\sum_{m=1}^M\sqrt{p_{mk}}\mathbf{H}^H_{mk}\hat{\mathbf{H}}_{mk}\right\} \\
&= \mathbb{E}\left\{\sum_{m=1}^M\sqrt{p_{mk}}\left(\sqrt{\beta_{mk}}e^{-j\phi_{mk}} + \sqrt{\lambda_{mk}}\mathbf{H}'^H_{mk}\right)\right. \\
&\left.\times\left[\sqrt{\beta_{mk}}e^{j\phi_{mk}} + \lambda_{mk}\sqrt{q_k}\tau_p\left(\sum_{i\in\mathcal{C}_k}\sqrt{q_i}\tau_p\sqrt{\lambda_{mi}}\mathbf{H}'_{mi} + \mathbf{W}^p_{mk}\right)\mathbf{A}_{mk}\right]\right\},
\end{aligned} \tag{50}$$

therefore,

$$\mathbf{G}_k = \sum_{m=1}^M\sqrt{p_{mk}}\left(A\beta_{mk} + \sqrt{\lambda_{mk}}\lambda_{mk}\tau_p\sqrt{q_k}\tau_p\sqrt{q_k}\sqrt{\lambda_{mk}}A\mathbf{I}_N\mathbf{A}_{mk}\right), \tag{51}$$

because

$$\mathbb{E}\left\{\mathbf{H}'^H_{mk}\mathbf{H}'_{mi}\right\} = \begin{cases} A\mathbf{I}_N, & i = k \\ 0, & i \neq k, \end{cases} \tag{52}$$

and $\mathbb{E}\{\mathbf{H}'^H_{mk}\mathbf{W}^p_{mk}\} = 0$ since they are independent. Therefore, $\mathbf{G}_k$ can be written as in (27).

To derive (28), we divide the summation over n into two components as follows:

$$\begin{aligned}
\mathbf{B}_k &= \mathbb{E}\left\{\sum_{m=1}^M\sum_{i=1}^K\mathbf{H}^H_{m,k}\mathbf{V}_{m,i}\mathbf{V}^H_{m,i}\mathbf{H}_{m,k}\right\} \\
&+ \mathbb{E}\left\{\sum_{m=1}^M\sum_{\substack{n=1\\n\neq m}}^M\sum_{i=1}^K\mathbf{H}^H_{m,k}\mathbf{V}_{m,i}\mathbf{V}^H_{n,i}\mathbf{H}_{n,k}\right\}
\end{aligned}$$

$$- \mathbf{G}_k\mathbf{G}_k^H + \sigma^2_{w_k^d}\mathbf{I}_N = \mathcal{T}_1 + \mathcal{T}_2 - \mathbf{G}_k\mathbf{G}_k^H + \sigma^2_{w_k^d}\mathbf{I}_N. \tag{53}$$

The first term can be derived as follows:

$$\mathcal{T}_1 = \sum_{m=1}^{M}\sum_{i=1}^{K} p_{mi}\mathbb{E}\left\{\mathbf{H}_{m,k}^H \hat{\mathbf{H}}_{m,i}\hat{\mathbf{H}}_{m,i}^H \mathbf{H}_{m,k}\right\} \tag{54}$$

$$= \sum_{m=1}^{M}\sum_{i=1}^{K} p_{mi}\mathbb{E}\Bigg\{\left(\sqrt{\beta_{mk}}e^{-j\phi_{mk}} + \sqrt{\lambda_{mk}}\mathbf{H}'^H_{mk}\right) \times\left[\sqrt{\beta_{mi}}e^{j\phi_{mi}} + \lambda_{mi}\sqrt{q_i}\tau_p\left(\sum_{k'\in\mathcal{C}_i}\sqrt{q_{k'}}\tau_p\sqrt{\lambda_{mk'}}\mathbf{H}'_{mk'} + \mathbf{W}^p_{mi}\right)\mathbf{A}_{mi}\right] \times\left[\sqrt{\beta_{mi}}e^{-j\phi_{mi}} + \lambda_{mi}\sqrt{q_i}\tau_p\mathbf{A}^H_{mi}\left(\sum_{k'\in\mathcal{C}_i}\sqrt{q_{k'}}\tau_p\sqrt{\lambda_{mk'}}\mathbf{H}'^H_{mk'} + \mathbf{W}^{pH}_{mi}\right)\right] \times\left(\sqrt{\beta_{mk}}e^{j\phi_{mk}} + \sqrt{\lambda_{mk}}\mathbf{H}'_{mk}\right)\Bigg\} \tag{55}$$

$$= \sum_{m=1}^{M}\sum_{i=1}^{K} p_{mi}\mathbb{E}\Bigg\{\left(\sqrt{\beta_{mk}}e^{-j\phi_{mk}} + \sqrt{\lambda_{mk}}\mathbf{H}'^H_{mk}\right) \times\left[\sqrt{\beta_{mi}}e^{j\phi_{mi}} + \lambda_{mi}\sqrt{q_i}\tau_p\left(\sum_{k'\in\mathcal{C}_i}\sqrt{q_{k'}}\tau_p\sqrt{\lambda_{mk'}}\mathbf{H}'_{mk'} + \mathbf{W}^p_{mi}\right)\mathbf{A}_{mi}\right] \times\left[\sqrt{\beta_{mi}}e^{-j\phi_{mi}} + \lambda_{mi}\sqrt{q_i}\tau_p\mathbf{A}^H_{mi}\left(\sum_{k'\in\mathcal{C}_i}\sqrt{q_{k'}}\tau_p\sqrt{\lambda_{mk'}}\mathbf{H}'^H_{mk'} + \mathbf{W}^{pH}_{mi}\right)\right] \times\left(\sqrt{\beta_{mk}}e^{j\phi_{mk}} + \sqrt{\lambda_{mk}}\mathbf{H}'_{mk}\right)\Bigg\} \tag{56}$$

$$= \sum_{m=1}^{M}\sum_{i=1}^{K} p_{mi}\Bigg[A^2N\beta_{mk}\beta_{mi} + \lambda_{mk}\lambda^2_{mi}q_i\tau_p^2\mathbb{E} \left\{\mathbf{H}'^H_{mk}\left(\sum_{k'\in\mathcal{C}_i}\sqrt{q_{k'}}\tau_p\sqrt{\lambda_{mk'}}\mathbf{H}'_{mk'} + \mathbf{W}^p_{mi}\right)\mathbf{A}_{mi}\mathbf{A}^H_{mi} \left(\sum_{k'\in\mathcal{C}_i}\sqrt{q_{k'}}\tau_p\sqrt{\lambda_{mk'}}\mathbf{H}'^H_{mk'} + \mathbf{W}^{pH}_{mi}\right)\mathbf{H}'_{mk}\right\}\Bigg] \tag{57}$$

$$= \sum_{m=1}^{M}\sum_{i=1}^{K} p_{mi}\Big[A^2N\beta_{mk}\beta_{mi} + \lambda_{mk}\lambda^2_{mi}q_i\tau_p^2(\mathcal{T}_{11} + \mathcal{T}_{12})\Big]. \tag{58}$$

The first subterm can be calculated on the basis of whether $k \in \mathcal{C}_i$ as follows:

$$\mathcal{T}_{11} = \begin{cases} \lambda_{mk}q_k\tau_p^2\mathbb{E}\left\{\mathbf{H}'^H_{mk}\mathbf{H}'_{mk}\mathbf{A}_{mi}\mathbf{A}^H_{mi}\mathbf{H}'^H_{mk}\mathbf{H}'_{mk}\right\} \\ + \sum_{\substack{k'\in\mathcal{C}_i \\ k'\neq k}} q_{k'}\tau_p^2\lambda_{mk'} \\ \times\mathbb{E}\left\{\mathbf{H}'^H_{mk}\mathbf{H}'_{mk'}\mathbf{A}_{mi}\mathbf{A}^H_{mi}\mathbf{H}'^H_{mk'}\mathbf{H}'_{mk}\right\}, & k \in \mathcal{C}_i \\ \sum_{k'\in\mathcal{C}_i} q_{k'}\tau_p^2\lambda_{mk'} \\ \times\mathbb{E}\left\{\mathbf{H}'^H_{mk}\mathbf{H}'_{mk'}\mathbf{A}_{mi}\mathbf{A}^H_{mi}\mathbf{H}'^H_{mk'}\mathbf{H}'_{mk}\right\}, & k \notin \mathcal{C}_i. \end{cases} \tag{59}$$

Therefore,

$$\mathcal{T}_{11} = \begin{cases} \left(3\tau_p^2q_k\lambda_{mk} + \sum_{\substack{k'\in\mathcal{C}_i \\ k'\neq k}} q_{k'}\tau_p^2\lambda_{mk'}\right) \\ \times AN\mathrm{tr}\left(\mathbf{A}_{mi}\mathbf{A}^H_{mi}\right), & k \in \mathcal{C}_i \\ \sum_{\substack{k'\in\mathcal{C}_i \\ k'\neq k}} q_{k'}\tau_p^2\lambda_{mk'}AN\mathrm{tr}\left(\mathbf{A}_{mi}\mathbf{A}^H_{mi}\right), & k \notin \mathcal{C}_i. \end{cases} \tag{60}$$

The other subterm can be derived as follows:

$$\mathcal{T}_{12} = \mathbb{E}\left\{\mathbf{H}'^H_{mk}\mathbf{W}^p_{mi}\mathbf{A}_{mi}\mathbf{A}^H_{mi}\mathbf{W}^{pH}_{mi}\mathbf{H}'_{mk}\right\} \tag{61}$$

$$= AN\sigma^2_{wp}\mathrm{tr}\left(\mathbf{A}_{mi}\mathbf{A}^H_{mi}\right)\mathbf{I}_N. \tag{62}$$

Accordingly, compensating from (60) and (62) into (58) gives (29).

The second term of $\mathbf{B}_k$, $\mathcal{T}_2$, can be derived as follows:

$$\mathcal{T}_2 = \mathbb{E}\left\{\sum_{m=1}^{M}\sum_{\substack{n=1 \\ n\neq m}}^{M}\sum_{i=1}^{K}\sqrt{p_{mi}p_{ni}}\mathbf{H}^H_{m,k}\hat{\mathbf{H}}_{m,i}\hat{\mathbf{H}}^H_{n,i}\mathbf{H}_{n,k}\right\} \tag{63}$$

$$= \sum_{m=1}^{M}\sum_{\substack{n=1 \\ n\neq m}}^{M}\sum_{i=1}^{K}\sqrt{p_{mi}p_{ni}}\mathbb{E}\Bigg\{\left(\sqrt{\beta_{mk}}e^{-j\phi_{mk}} + \sqrt{\lambda_{mk}}\mathbf{H}'^H_{mk}\right) \times\left[\sqrt{\beta_{mi}}e^{j\phi_{mi}} + \lambda_{mi}\sqrt{q_i}\tau_p\left(\sum_{k'\in\mathcal{C}_i}\sqrt{q_{k'}}\tau_p\sqrt{\lambda_{mk'}}\mathbf{H}'_{mk'} + \mathbf{W}^p_{mi}\right)\mathbf{A}_{mi}\right] \times\left[\sqrt{\beta_{ni}}e^{-j\phi_{ni}} + \lambda_{ni}\sqrt{q_i}\tau_p\mathbf{A}^H_{ni}\left(\sum_{k'\in\mathcal{C}_i}\sqrt{q_{k'}}\tau_p\sqrt{\lambda_{nk'}}\mathbf{H}'^H_{nk'} + \mathbf{W}^{pH}_{ni}\right)\right] \times\left(\sqrt{\beta_{nk}}e^{j\phi_{nk}} + \sqrt{\lambda_{nk}}\mathbf{H}'_{nk}\right)\Bigg\} \tag{64}$$

$$= \sum_{m=1}^{M}\sum_{\substack{n=1 \\ n\neq m}}^{M}\sum_{i=1}^{K}\sqrt{p_{mi}p_{ni}}\Big(\sqrt{\beta_{mk}\beta_{mi}\beta_{ni}\beta_{nk}} \times e^{-j\phi_{mk}}e^{j\phi_{mi}}e^{-j\phi_{ni}}e^{j\phi_{nk}}A^2N + \mathcal{T}_{21}\Big), \tag{65}$$

where,

$$\mathcal{T}_{21} = \begin{cases} \sqrt{\lambda_{mk}\lambda_{nk}}\lambda_{mi}\lambda_{ni}q_i\tau_p^2 \times \tau_p^2q_k\sqrt{\lambda_{mk}\lambda_{nk}} \\ \times\mathbb{E}\left\{\mathbf{H}'^H_{mk}\mathbf{H}'_{mk}\mathbf{A}_{mi}\mathbf{A}^H_{ni}\mathbf{H}'^H_{nk}\mathbf{H}'_{nk}\right\} \\ + \tau_p^2q_k\sqrt{\lambda_{mk}\lambda_{nk}} \\ \times\mathbb{E}\left\{\mathbf{H}'^H_{mk}\mathbf{W}^p_{mi}\mathbf{A}_{mi}\mathbf{A}^H_{ni}\mathbf{W}^{pH}_{ni}\mathbf{H}'_{nk}\right\}, & k \in \mathcal{C}_i \\ 0, & k \notin \mathcal{C}_i, \end{cases} \tag{66}$$

due to the independence of random variables. Therefore,

$$\mathcal{T}_{21} = \begin{cases} \lambda_{mk}\lambda_{nk}\lambda_{mi}\lambda_{ni}q_i^2\tau_p^4A^2\mathbf{A}_{mi}\mathbf{A}^H_{ni}, & k \in \mathcal{C}_i \\ 0, & k \notin \mathcal{C}_i. \end{cases} \tag{67}$$

Accordingly, compensating from (67) into (65) gives (30). ■

REFERENCES

[1] F. Rinaldi et al., "Non-terrestrial networks in 5G & beyond: A survey," *IEEE Access*, vol. 8, pp. 165178–165200, 2020.

[2] "Study on new radio (NR) to support non-terrestrial networks (release 15)," 3GPP, Sophia Antipolis, France, Rep. TR 38.811, V15.4.0, Sep. 2020.

[3] "Study on using satellite access in 5G (release 16)," 3GPP, Sophia Antipolis, France, Rep. TR 22.822, V16.0.0, Jun. 2018.

[4] "Study on management and orchestration aspects with integrated satellite components in a 5G network (release 17)," 3GPP, Sophia Antipolis, France, Rep. TR 28.808, V17.0.0, Mar. 2021.

[5] "Study on architecture aspects for using satellite access in 5G (release 17)," 3GPP, Sophia Antipolis, France, Rep. TR 23.737, V17.2.0, Mar. 2021.
[6] "Solutions for NR to support non-terrestrial networks (release 16)," 3GPP, Sophia Antipolis, France, Rep. TR 38.821, V16.1.0, Jun. 2021.
[7] "Advanced plans for 5G." Accessed: Aug. 1, 2022. [Online]. Available: https://www.3gpp.org/news-events/2210-advanced_5g
[8] G. Araniti, A. Iera, S. Pizzi, and F. Rinaldi, "Toward 6G non-terrestrial networks," *IEEE Netw.*, vol. 36, no. 1, pp. 113–120, Jan./Feb. 2022.
[9] M. Y. Abdelsadek et al., "Future space networks: Toward the next giant leap for humankind," *IEEE Trans. Commun.*, vol. 71, no. 2, pp. 949–1007, Feb. 2023.
[10] R. Gopal and N. BenAmmar, "Framework for unifying 5G and next generation satellite communications," *IEEE Netw.*, vol. 32, no. 5, pp. 16–24, Sep./Oct. 2018.
[11] K. Maine, C. Devieux, and P. Swan, "Overview of IRIDIUM satellite network," in *Proc. IEEE WESCON*, 1995, pp. 483–490.
[12] "Space startup Lynk uses satellite to send text message to unmodified android phone." Accessed: Aug. 1, 2022. [Online]. Available: https://lynk.world/news#:~:text=Space%20startup%20Lynk, connectivity%20from%20orbit
[13] E. G. Larsson, O. Edfors, F. Tufvesson, and T. L. Marzetta, "Massive MIMO for next generation wireless systems," *IEEE Commun. Mag.*, vol. 52, no. 2, pp. 186–195, Feb. 2014.
[14] F. Völk, R. T. Schwarz, and A. Knopp, "Multi-user MIMO satellite communications for aviation networks," in *Proc. EEE 93rd Veh. Technol. Conf. (VTC-Spring)*, 2021, pp. 1–7.
[15] R. T. Schwarz, T. Delamotte, K.-U. Storek, and A. Knopp, "MIMO applications for multibeam satellites," *IEEE Trans. Broadcast.*, vol. 65, no. 4, pp. 664–681, Dec. 2019.
[16] P.-D. Arapoglou, K. Liolis, M. Bertinelli, A. Panagopoulos, P. Cottis, and R. De Gaudenzi, "MIMO over satellite: A review," *IEEE Commun. Surveys Tuts.*, vol. 13, no. 1, pp. 27–51, 1st Quart., 2010.
[17] R. Schwarz, A. Knopp, and B. Lankl, "The channel capacity of MIMO satellite links in a fading environment: A probabilistic analysis," in *Proc. Int. Workshop Satell. Space Commun.*, 2009, pp. 78–82.
[18] P.-D. Arapoglou, P. Burzigotti, M. Bertinelli, A. B. Alamanac, and R. De Gaudenzi, "To MIMO or not to MIMO in mobile satellite broadcasting systems," *IEEE Trans. Wireless Commun.*, vol. 10, no. 9, pp. 2807–2811, Sep. 2011.
[19] C. Hofmann, K.-U. Storek, R. T. Schwarz, and A. Knopp, "Spatial MIMO over satellite: A proof of concept," in *Proc. IEEE Int. Conf. Commun. (ICC)*, 2016, pp. 1–6.
[20] L. You, K.-X. Li, J. Wang, X. Gao, X.-G. Xia, and B. Ottersten, "Massive MIMO transmission for LEO satellite communications," *IEEE J. Sel. Areas Commun.*, vol. 38, no. 8, pp. 1851–1865, Aug. 2020.
[21] K.-X. Li et al., "Downlink transmit design for massive MIMO LEO satellite communications," *IEEE Trans. Commun.*, vol. 70, no. 2, pp. 1014–1028, Feb. 2022.
[22] L. You, K.-X. Li, J. Wang, X. Gao, X.-G. Xia, and B. Otterstenx, "LEO satellite communications with massive MIMO," in *Proc. IEEE Int. Conf. Commun. (ICC)*, Jun. 2020, pp. 1–6.
[23] J. Palacios, N. Gonzalez-Prelcic, C. Mosquera, T. Shimizu, and C.-H. Wang, "A hybrid beamforming design for massive MIMO LEO satellite communications," 2021, *arXiv:2104.11158*.
[24] X. Qiang et al., "Hybrid A/D precoding for downlink massive MIMO in LEO satellite communications," in *Proc. IEEE Int. Conf. Commun. Workshops (ICC Workshops)*, 2021, pp. 1–6.
[25] C. Liao, K. Xu, H. Zhu, X. Xia, Q. Su, and N. Sha, "Secure transmission in satellite-UAV integrated system against eavesdropping and jamming: A two-level Stackelberg game model," *China Commun.*, vol. 19, no. 7, pp. 53–66, Jul. 2022.
[26] R. Richter, I. Bergel, Y. Noam, and E. Zehavi, "Downlink cooperative MIMO in LEO satellites," *IEEE Access*, vol. 8, pp. 213866–213881, 2020.
[27] H. Q. Ngo, A. Ashikhmin, H. Yang, E. G. Larsson, and T. L. Marzetta, "Cell-free massive MIMO versus small cells," *IEEE Trans. Wireless Commun.*, vol. 16, no. 3, pp. 1834–1850, Mar. 2017.
[28] S. Elhoushy, M. Ibrahim, and W. Hamouda, "Cell-free massive MIMO: A survey," *IEEE Commun. Surveys Tuts.*, vol. 24, no. 1, pp. 492–523, 1st Quart., 2021.
[29] M. Y. Abdelsadek, H. Yanikomeroglu, and G. K. Kurt, "Future ultra-dense LEO satellite networks: A cell-free massive MIMO approach," in *Proc. IEEE Int. Conf. Commun. Workshops (ICC Workshops)*, Jun. 2021, pp. 1–6.
[30] M. Y. Abdelsadek, G. K. Kurt, and H. Yanikomeroglu, "Distributed massive MIMO for LEO satellite networks," *IEEE Open J. Commun. Soc.*, vol. 3, pp. 2162–2177, 2022.
[31] J. Amadid, M. Boulouird, A. Belhabib, and A. Zeroual, "On channel estimation for Rician fading with the phase-shift in cell-free massive MIMO system," *Wireless Personal Commun.*, vol. 124, no. 3, pp. 1923–1943, 2022.
[32] Y. Zhang, Y. Wu, A. Liu, X. Xia, T. Pan, and X. Liu, "Deep learning-based channel prediction for LEO satellite massive MIMO communication system," *IEEE Wireless Commun. Lett.*, vol. 10, no. 8, pp. 1835–1839, Aug. 2021.
[33] E. Björnson, J. Hoydis, and L. Sanguinetti, "Massive MIMO networks: Spectral, energy, and hardware efficiency," *Found. Trends Signal Process.*, vol. 11, nos. 3–4, pp. 154–655, 2017.
[34] Y. Zhang, A. Liu, P. Li, and S. Jiang, "Deep learning (DL)-based channel prediction and hybrid beamforming for LEO satellite massive MIMO system," *IEEE Internet Things J.*, vol. 9, no. 23, pp. 23705–23715, Dec. 2022.
[35] L. Pan, T. Jiang, L. Zhou, H. Xu, and W. Chen, "A research on high-precision time-synchronization and ranging system between satellites," in *Proc. Int. Conf. Microw. Millimeter Wave Technol.*, vol. 2, 2008, pp. 926–929.
[36] W. Tushar, D. B. Smith, A. Zhang, T. A. Lamahewa, and T. Abhayapala, "Distributed transmit beamforming: Phase convergence improvement using enhanced one-bit feedback," in *Proc. IEEE Wireless Commun. Netw. Conf. (WCNC)*, 2012, pp. 528–532.
[37] S. B. Amor, S. Affes, F. Bellili, U. Vilaipornsawai, L. Zhang, and P. Zhu, "Multi-node ML time and frequency synchronization for distributed MIMO-relay beamforming over time-varying flat-fading channels," *IEEE Trans. Commun.*, vol. 67, no. 4, pp. 2702–2715, Apr. 2019.
[38] S. Buzzi and C. D'Andrea, "Cell-free massive MIMO: User-centric approach," *IEEE Wireless Commun. Lett.*, vol. 6, no. 6, pp. 706–709, Dec. 2017.
[39] A. U. Chaudhry and H. Yanikomeroglu, "Free space optics for next-generation satellite networks," *IEEE Consum. Electron. Mag.*, vol. 10, no. 6, pp. 21–31, Nov. 2021.

MOHAMMED Y. ABDELSADEK (Senior Member, IEEE) received the B.Sc. (Hons.) and M.Sc. degrees in electrical and computer engineering from Assiut University, Assiut, Egypt, in 2011 and 2014, respectively, and the Ph.D. degree in electrical and computer engineering from the Memorial University of Newfoundland, St. John's, NL, Canada, in 2020. He is currently a Postdoctoral Fellow with Carleton University, Ottawa, ON, Canada. He is also an Assistant Professor (on leave) with the Department of Electrical Engineering, Assiut University. Earlier, he was a Sessional Instructor with the Memorial University of Newfoundland. His current research interests include satellite communication networks, ultra-reliable low-latency communications, radio resource management, and AI/ML for wireless networks. He has served as a reviewer and a TPC member for several IEEE journals and conferences.

GUNES KARABULUT-KURT (Senior Member, IEEE) received the B.S. degree with (high Hons.) in electronics and electrical engineering from Boğaziçi University, Istanbul, Turkey, in 2000, and the M.A.Sc. and the Ph.D. degrees in electrical engineering from the University of Ottawa, ON, Canada, in 2002 and 2006, respectively. From 2000 to 2005, she was a Research Assistant with the CASP Group, University of Ottawa. She was with TenXc Wireless, Canada, from 2005 to 2006, Edgewater Computer Systems Inc., Canada, from 2006 to 2008, Turkcell Research and Development Applied Research and Technology, Istanbul, from 2008 to 2010, and Istanbul Technical University from 2010 and 2021. She is currently an Associate Professor of Electrical Engineering with Polytechnique Montréal, Montréal, QC, Canada. In addition, she is an Adjunct Research Professor with Carleton University. She has received the Turkish Academy of Sciences Outstanding Young Scientist (TÜBA-GEBIP) Award in 2019. She is currently serving as an Associate Technical Editor of the *IEEE Communications Magazine*, an Associate Editor of IEEE COMMUNICATION LETTERS, an Associate Editor of IEEE WIRELESS COMMUNICATIONS LETTERS, and an Area Editor of IEEE TRANSACTIONS ON MACHINE LEARNING IN COMMUNICATIONS AND NETWORKING. She is serving as the Secretary of IEEE Satellite and Space Communications Technical Committee and also the Chair of the IEEE special interest group titled "Satellite Mega-Constellations: Communications and Networking". She is a Distinguished Lecturer of Vehicular Technology Society Class of 2022. She is a Marie Curie Fellow and a member of the IEEE WCNC Steering Board.

HALIM YANIKOMEROGLU (Fellow, IEEE) received the B.Sc. degree in electrical and electronics engineering from Middle East Technical University, Ankara, Turkey, in 1990, and the M.A.Sc. degree in electrical engineering (currently ECE) and the Ph.D. degree in electrical and computer engineering from the University of Toronto, Canada, in 1992 and 1998, respectively.

Since 1998, he has been with the Department of Systems and Computer Engineering, Carleton University, Ottawa, Canada, where he is currently a Full Professor. He has given 110+ invited seminars, keynotes, panel talks, and tutorials in the last five years. He has supervised or hosted over 150 postgraduate researchers in his lab at Carleton. His extensive collaborative research with industry resulted in 39 granted patents. His research interests cover many aspects of wireless communications and networks, with a special emphasis on non-terrestrial networks in the recent years.

Dr. Yanikomeroglu received several awards for his research, teaching, and service, including the IEEE ComSoc Fred W. Ellersick Prize in 2021, the IEEE VTS Stuart Meyer Memorial Award in 2020, and the IEEE ComSoc Wireless Communications TC Recognition Award in 2018. He received best paper awards at IEEE Competition on Non-Terrestrial Networks for B5G and 6G in 2022 (Grand Prize), the IEEE ICC 2021, and the IEEE WISEE 2021 and 2022. He is currently serving as the Chair of the Steering Committee of IEEE's Flagship Wireless event, Wireless Communications and Networking Conference. He is also a member of the IEEE ComSoc Governance Council, IEEE ComSoc GIMS, IEEE ComSoc Conference Council, and IEEE PIMRC Steering Committee. He has served as the general chair and the technical program chair of several IEEE conferences. He has also served in the editorial boards of various IEEE periodicals. He is a Distinguished Speaker for the IEEE Communications Society and the IEEE Vehicular Technology Society, and an Expert Panelist of the Council of Canadian Academies. He is a Fellow of the Engineering Institute of Canada and the Canadian Academy of Engineering.

PENG HU (Senior Member, IEEE) received the Ph.D. degree in electrical engineering from Queen's University, Canada. He is currently a Research Officer with the National Research Council Canada and an Adjunct Professor with the Cheriton School of Computer Science, University of Waterloo. His current research interests include satellite-terrestrial integrated networks, autonomous networking, and industrial Internet of Things systems. He has served as an Associate Editor of the IEEE CANADIAN JOURNAL OF ELECTRICAL AND COMPUTER ENGINEERING, a Voting Member of the IEEE Sensors Standards committee, and on the Organizing/Technical Committees of Industry Consortia and International Conferences/Workshops at IEEE ICC'23, IEEE GLOBECOM'21, IEEE PIMRC'17, and IEEE AINA'15.

GUILLAUME LAMONTAGNE received the B.Eng. and M.Eng. degrees from the École de Technologie Supérieure, Montreal, QC, Canada, in 2007 and 2009, respectively. His experience in satellite communications started through internships and research activities with the Canadian Space Agency, in 2005; and the Centre national d'études spatiales, France, in 2006 and 2008. In 2009, he joined MDA and held various communication systems engineering and management positions before being appointed as the Director of Technology, Payloads, in 2019 and then the Director of Technology Strategy, Satellite Systems in 2021. Through this role, he is leading MDA's research and development activities for satellite communications as well as establishing the related long-term development strategy.

KHALED AHMED received the B.S. and M.Sc. degrees in wireless communications from Cairo University, Egypt, in 2010 and 2015, respectively, and the Ph.D. degree in optical communications from McMaster University, Canada, in 2019. He was a Postdoctral Fellow of Machine Learning for Resource-Limited Devices with McMaster University, Canada, in 2021. He is currently working as a Member Technical Staff II with the Systems Engineering Department, MDA, Sainte-Anne-de Bellevue, QC, Canada. His current research interests include RF and optical communications for terrestrial and satellite networks, optical beamforming networks, and applied machine learning and deep learning in networks.